Metal-free activated biochar as an oxygen reduction reaction catalyst in single chamber microbial fuel cells

Tommy Pepè Sciarria[a1], Maida Aysla Costa de Oliveira[b1], Barbara Mecheri[b], Alessandra D'Epifanio[b], Jillian L. Goldfarb[c], Fabrizio Adani [a]*

[a]Gruppo ricicla lab., Disaa, University of Milan, via Celoria 2, 20133, Italy
[b]Department of Chemical Science and Technologies, University of Rome Tor Vergata, Via della Ricerca Scientifica, 00133, Rome, Italy
[c]Department of Biological and Environmental Engineering, College of Agriculture and Life Sciences, Cornell University, Ithaca, NY 14853, USA.

*Corresponding Authors: fabrizio.adani@unimi.it
[1]These Authors contributed equally to the work

Abstract

Metal-free catalysts are promising candidates for Bio-electrochemical Systems (BESs) due to their high surface area, chemical stability, good electrical conductivity, and enhanced mass-transport capabilities. In this study, biochars derived from olive mill waste (OMW) with and without supercritical CO_2 pretreatment, and salted pistachio nut shells, were produced via pyrolysis and/or chemical and physical activation. The catalytic activity towards oxygen reduction reactions (ORR) of the biochars was investigated by cyclic and linear sweep voltammetry in neutral media. The electrochemical characterization of the samples revealed that olive mill waste biochar showed the highest catalytic activity toward ORR, in terms of reaction rate (Epr V vs. RHE= 0.537± 0.00), density of active sites, and number of electrons exchanged (ne- $E_{@}$ -0.6 V vs. RHE=3.9±0.2). These biochars were

used as catalysts in air cathode microbial fuel cells. The power density obtained by MFCs equipped with an OMW cathode achieved a maximum power density of 271 ± 34 mWm^{-2} (R_{ext}=250 Ω). This value was approximately 15 times higher than the power density obtained by a commercial carbon black used as control.

Graphical Abstract

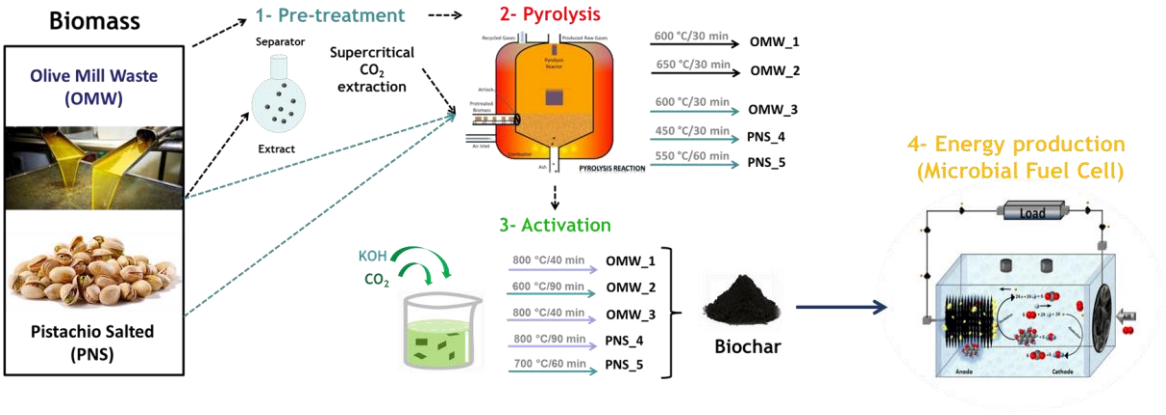

Keywords: Olive mill waste; pistachio nutshell; biochar; activated carbon; Oxygen reduction reaction; Microbial fuel cell.

1. Introduction

In recent years, biomasses sourced from agricultural by-products have been touted as an important feedstock for the production of high-value materials, chemicals, and fuels to promote a circular economy and zero-waste production [1]. Within the wide range of possible products recoverable from biomass, the conversion of residual carbon to upgraded biochars that serve as high performance materials for electrochemical energy systems represents a sustainable and economic green energy application [2]. Many electrochemical storage and conversion systems use carbon electrodes, often composed of different types

of nanostructured carbon materials having high surface area and porosity, high electrical and thermal conductivity, high stability, low cost and abundant availability [3,4]. There are many different types of energy conversion devices that use biochars for electrode materials. One example is microbial fuel cells (MFCs), which oxidize biodegradable organics in aqueous wastes by electrochemically active microorganisms while generating renewable electricity. By using this technology, it is possible to harvest energy in the form of electricity, using domestic wastes and wastewaters as a fuel, reducing at the same time the problems linked to their disposal.

The performance of MFCs is highly influenced by reactions on the cathode side [5], where oxygen is the most widely used electron acceptor in air-cathode MFCs. Nevertheless, the oxygen reduction reaction (ORR) at the cathode is one of the major challenges limiting the MFC due to the high over potential and slow reaction kinetics under normal MFC operating conditions [3]. Precious metal catalysts, such as platinum group metals, are extensively used to enhance ORR kinetics. However, Pt/C catalysts, which are the state-of-the-art catalyst for conventional fuel cells, are not suitable for large scale application in MFCs due to platinum's limited reserves, high cost and sensitivity to poisoning [6]. As such, the inclusion of non-precious materials such as graphene and nanostructured carbons represent both a sustainable and more economically viable catalyst for MFCs [7,8,9]. In recent years, biochars made from the pyrolysis and subsequent activation of a variety of biomasses have been explored as low-cost catalysts to replace platinum group metals in MFCs due to their good electric conductivity and enhanced mass transport capability [10,11].

A handful of prior studies report the use of the low-cost biochar from agricultural biomass by-products such as coconut shell and banana peels [12] as well as sewage sludge [13] as

ORR electrocatalysts for MFC cathodes. The present work explores the suitability of various preparation conditions on the catalytic activity of olive mill waste (OMW) and pistachio nutshell (PNS) derived activated biochars for ORR electrocatalyst for MFC cathodes. Olive mill waste and pistachio nutshells are widely available agricultural by products: OMW reached a global production of 3×10^7 m^3 per year [14] and has a high disposal cost associated with this production [14,15]. Worldwide pistachio production amounts to over 5.8×10^5 m^3 per year (in-shell basis) mainly produced in the United States, Iran and Turkey [16]. These two food production waste products were selected for their dense structures as well as intrinsically high content of heteroatoms, which are beneficial to increase current density and accelerate the ORR activity [17,18].

In this study, activated biochars derived from olive mill waste and pistachio nutshells precursors were produced by several facile, low-cost, and readily scalable thermochemical approaches. The catalytic activity of the activated biochars towards ORR was investigated by cyclic and linear sweep voltammetry in neutral media. The ORR activity of the fabricated biochar-based activated carbons was probed via the assembly of biochar-based cathodes in single chamber MFC to evaluate electrochemical performance in terms of power generation and coulombic efficiency.

2. Materials and Methods

An initial set of five activated biochars from two biomass precursors were manufactured and their baseline electrochemical performance assessed. From this analysis, two biochars were selected for inclusion in a microbial fuel cell to compare their ORR activity against a commercial activated carbon.

2.1 Synthesis of Biochar catalysts

Biomass Samples

Olive mill waste was sourced from an olive oil production plant in Calabria, Italy. A portion of the waste was supercritical fluid extracted as previously described [17]. Briefly, raw olive mill waste (OMW) was extracted with pure supercritical CO_2 (SCO_2) at a total pressure of 250 bar and a temperature of 70 °C, with a CO_2 flow rate of 80 $kg \cdot hr^{-1}$. The reactor contained 7300 g of raw OMW. To achieve a uniform particle size, the OMW raw and SCO_2 samples were ground in a ball mill and mechanically sieved, which yielded sufficient quantities of particles between 250 and 300 μm.

Salted pistachio nuts were purchased from Trader Joe's (product of California, USA) and the shells and nutmeat separated. The shells were weighed to the 0.1 mg, then washed in deionized water and placed into an oven at 90°C to dry, and the weight recorded. This procedure was repeated three times until a constant weight was obtained to remove all traces of salt. The shells were ground and sieved to a particle fraction between 125 and 300 μm.

Preparation of Activated Biochars

CO_2-activated biochars were prepared in a 2" MTI tube furnace. Approximately 10 g of the raw or extracted OMW or PNS sample was loaded into a porcelain boat and inserted into the quartz tube. The samples were heated under 100 mL/min of high purity nitrogen to 110 °C at 10 °C/min and held for 30 minutes to remove residual moisture, then to 600°C (OMW) or 450/550°C (PNS; conditions given in Table 1) and held for 30 min to pyrolyze a portion of the volatile matter. Following this brief pyrolysis step, the samples were then

heated at a rate of 10 °C min^{-1} to 800 °C, at which point high purity CO_2 at 100 mL/min was introduced into the reactor bed, and the sample was held at 800 °C under CO_2 for 45 minutes (OMW samples) or 90 minutes (PNS samples) to produce the physically activated biochars. It was found that 90 minutes resulted in considerable oxidation for the OMW samples, whereas 45 minutes was not sufficient to open the porous network for the PNS samples. Following CO_2 treatment, the samples were cooled in an inert atmosphere to room temperature.

Chemical activation of the biomass samples was performed using potassium hydroxide (KOH), a known porogen. To achieve sufficient porosity development while maintaining structural integrity, the biomasses were first pyrolyzed (conditions given in Table 1) and then subjected to chemical treatment. The KOH was dissolved in deionized water at a weight ratio of 14:1 H_2O: KOH. Raw biomass in a ratio of 2:1 KOH: biomass was added to the beaker and the contents stirred at 150 rpm for one hour. The soaked samples were filtered and washed with 3 volumes of 150 mL each of deionized water, then dried, uncovered, in a laboratory oven at 110 °C. Samples were subsequently activated in the tube furnace under nitrogen at 600 °C (OMW samples) or 700°C (PNS samples) at a heating rate of 10 °C min^{-1} with a 60 minute hold time, and cooled under N_2 to prevent oxidation. After being removed from the tube furnace, the samples were neutralized with 1.2 M HCl; the pH of the filtrate was monitored using pH paper until it was between 7.2 and 6.7. The samples were washed once more with 150 mL of DI water and gravimetrically filtered, then dried overnight. These dried activated samples were flushed once more with deionized water to remove any visible traces of salt that had crystallized and were then filtered. The

chemically activated solid collected on the filter paper was dried, uncovered, in the oven overnight at 110 °C.

A synoptic scheme is reported in Table 1.

Table 1: Samples labeling of biochars obtained from two different types of biomass, and experimental condition for their synthesis and activation.

Feedstock biomass	**Synthesis and Activation**			**Sample labeling**
	Pretreatment	**Pyrolysis**	**Activation**	
Olive Mill Waste (OMW)	Supercritical CO_2 extraction	600 °C, 30 min.	CO_2 (45 min. 800 °C)	OMW_1
	Supercritical CO_2 extraction	600 °C, 30 min.	KOH (60 min. 600 °C)	OMW_2
	none	600 °C, 30 min.	CO_2 (45 min. 800 °C)	OMW_3
Pistachio Nutshells (PNS)	Washed	450 °C, 30 min.	CO_2 (90 min. 800 °C)	PNS_4
	Washed	550 °C, 60 min.	KOH (60 min. 700 °C)	PNS_5

2.2 Biochar characterization and electrochemical performance assessment

To down select a series of activated biochars to manufacture in greater quantity and use for MFC studies, a series of physical, chemical and electrochemical measurements were obtained on each of the biochars listed in Table 1.

Biochar Physical and Chemical Characteristics

The carbon content (volatile + fixed carbon) was determined in a Mettler Toledo TGA/DSC-1 by heating 9-11 mg of each sample in a 70 μL alumina crucible at 10°C/min under 50 mL/min air to 110 °C and held for 30 minutes to remove residual moisture.

Samples were then oxidized in air heated at 10°C/min up to 900 °C, held for 60 minutes with the loss attributed to total carbon content. The ultimate analysis was conducted in an Exeter Analytical CE-4400 Elemental Analyzer to measure C, H, N; O was determined by difference. Both carbon content and elemental analyses were repeated twice; results presented are the average of two runs, all of which were within ± 2% for each sample. The BET surface area of the samples was measured on a Quantachrome Autosorb-1 over a partial pressure range of 0 to 0.35 using nitrogen as the adsorbate gas. Samples were degassed prior to measurement for at least 16 hours at 180 °C.

Fourier transform infrared spectroscopy (FTIR) was carried out using a FTIR100 spectrometer (Perkin Elmer) in transmittance mode to assess the biochars' surface functional groups. Biochar samples were pelleted in 150 mg of KBr (at 0.5 wt.% loading) using a Specac manual hydraulic press, by applying a pressure of 7 tons for 5 min. The diameter of pellets was of 13 mm.

Biochar morphology was characterized using scanning electron microscopy (SEM) using a field emission SEM microscope (FE-SEM, SUPRA™ 35, Carl Zeiss SMT, Oberkochen, Germany), by dropping a 1 mg mL^{-1} dispersion of biochar in ethanol on carbon tape (5.00 kV beam voltage; magnification 50.00 and 10.00 KX).

Electrochemical Characterization

Cyclic voltammetry (CV) and linear sweep voltammetry (LSV) with rotating disk electrode (RDE) were performed in three electrodes cells. The reference electrode was a saturated calomel electrode (SCE, Amel 303/SCG/12), the auxiliary electrode was a platinum wire

(Amel, 805/SPG/12), and the working electrode (WE) was a glassy carbon disk (GC, 0.196 cm^2 area) modified with the catalyst layer.

The electrolyte solution was a 0.1 M neutral phosphate buffer solution, saturated in either nitrogen or oxygen atmosphere at room temperature. The catalyst layer was prepared by dispersing 4 mg of biochar in 270 µL of distilled water, 135 µL of ethanol, and 50 µL of a Nafion® perfluorinated resin solution (274704, Aldrich). Then the mixture was treated in an ultrasonic bath for 30 min and deposited on the GC electrode to achieve a catalyst loading of 0.3 mg cm^{-2}. The GC electrode was dried at 70 °C for 2 min. under vacuum.

CV was run between -0.9 V and 0.6 V with a scan rate of 5 mVs^{-1}. The electrical double-layer capacitance, C_{DL}, of biochars was estimated by acquiring CV curves in N_2-saturated atmosphere and measuring the charging current in the absence of Faradic contribution (at -0.1 V) as a function of potential scan rate from 5 to 50 mVs^{-1}. A capacitance of 30 µF cm^2 was used to estimate the electrochemical surface area (ECSA) [19-23] LSV-RDE experiments were run between -0.8 V and 0.2 V at 5 mVs^{-1} under hydrodynamic conditions, with electrode rotation speed in the range 100-1600 rpm. LSVs shown in this manuscript were corrected by subtracting the background current measured in a N_2 atmosphere. The overall number of electrons (n) exchanged in ORR (oxygen reduction reaction) were extrapolated by analyzing the LSV-RDE curves with the Koutecky–Levich theory, as previously reported [4, 24].

2.3 Preparation of MFC cathodes

The best performing biochars were incorporated into gas diffusion layer cathodes and then tested in microbial fuel cells. The cathodes were prepared as follows. Carbon cloth

electrodes (ELAT® LT1400W MPL treated, *FuelCellsEtc*, US) were modified by brush painting a PTFE diffusion layer on the opposite side of MPL, as previously described [3]. After that, the biochar layer was applied on the opposite side of the PTFE layer side by brush painting a 0.185 $mgmL^{-1}$ suspension of biochar in a solution of 2-propanol (31 vol.%), DI (7.5 vol.%), and Nafion® perfluorinated resin solution (274704, Aldrich, 61.5 vol.%): The loading of biochar was 5 $mgcm^{-2}$. The electrodes were dried at room temperature overnight and finally pressed at 90 °C for 2 min. at 2 bars.

Cathodes based on bare carbon black (Vulcan XC72R by Cabot corporation, MA, US) were also prepared and taken as a reference, with the same loading as compared to biochar-based cathodes. Carbon black was activated in concentrated nitric acid before use, as previously reported [25].

2.4 Operating conditions of MFCs

Microbial fuel cell experiments were performed using lab-scale prototypes of single chamber air-cathode MFCs with a volume of 28 mL, constructed by assembling the modified cathodes equipped with OMW_2 and OMW_3 as catalysts and commercial carbon black as a control (CTRL). The anode was made of graphite fibre brush with titanium wire as the core (Panex 33 160 K, Zoltek, US), 2.5 cm in both outer diameter and length. The estimated surface area was $0.22m^2$ or 18 200 m^2/m^3 brush-volume, the porosity being 95%. The fibre brush electrodes were heated at 450°C for 30 min under ambient air before use [5]. The tests were run by adding a synthetic solution of phosphate buffer solution (PBS) with neutral media pH and concentration of 0.1 M, containing 1 gL^{-1} sodium acetate, and acquiring voltage power generation cycles, as previously reported [5].

Polarization and power density curves were carried out by varying the external resistance (from 10 to 10 KΩ) every 30 min and measuring cell voltage at each resistance. Coulombic efficiency (CE), i.e. the fraction of electrons recovered as current versus that in the starting organic matter, was calculated as follows:

$$CE = Cp/CTi \times 100\% \quad [1]$$

where Cp is the total Coulombs calculated by integrating the current over time, CT_i is the theoretical amount of Coulombs that can be produced from the substrate, i.e. sodium acetate ($i = a$), calculated as:

$$CTi = Fb_iS_iv/M_i \quad [2]$$

In Equation 2, F is Faraday's constant (96 485 C/mol electrons), b_i the number of moles of electrons produced per mole of substrate (b acetate = 8), S_i the substrate concentration, and M_i the molecular weight of the substrate (M sodium acetate = 82) and v is the volume of the reactor. All measurements were carried out at room temperature (23 ± 3 °C) having two independent replicates for each cathode.

3. Results and Discussion

The morphology, physical surface area and surface functional groups of the five activated biochars produced were characterized prior to electrochemical performance assessments. Two biochars displaying optimized electrochemical performance were down selected for MFC performance assessment as compared to a commercial activated carbon.

3.1 Biochar characterization

The activated biochar samples have a heterogeneous morphology characterized by the presence of particle agglomerates and amorphous regions composed of different

microporous structures (Figure 1 and Figure S1). In particular, OMW samples have a granular profile with a porous structure, particularly evident for OMW_3 (Figure 1 a-b).

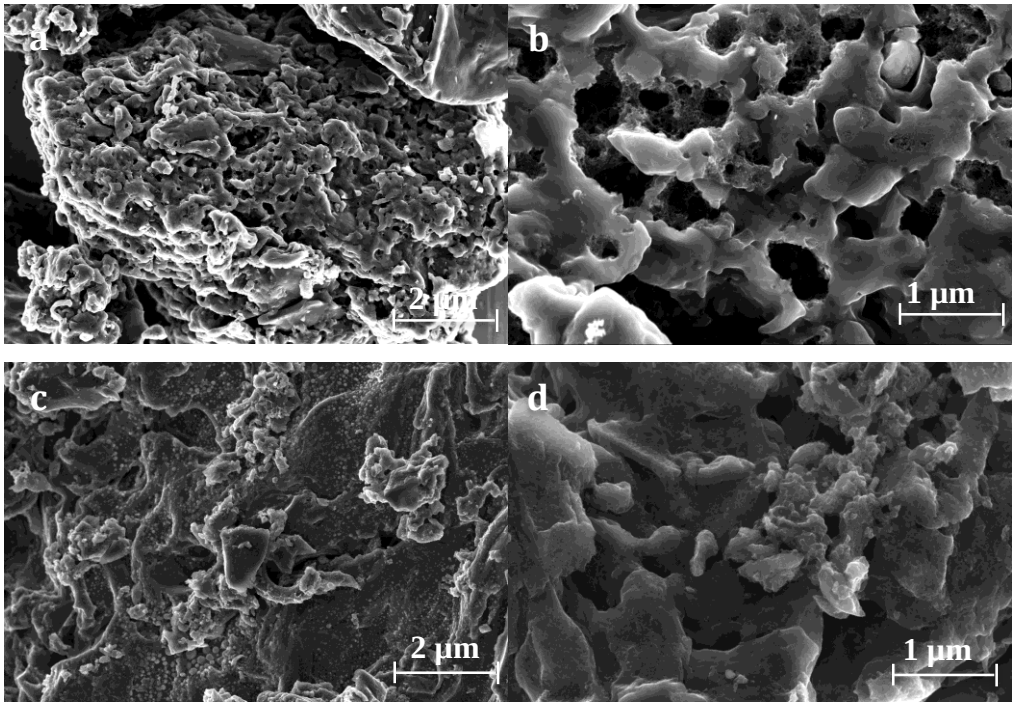

Figure 1: SEM images of biochars OMW_3 (a-b) and PNS_4 (c-d) at 10.00 KX and 50.00 KX magnification and EHT @ 5.00 KV.

Conversely, the granular profile and porous structure is less evident for the PNS samples (Figure 1 c-d), despite having a higher BET surface area than those of OMW biochar samples, as shown in Table 2. This finding can be ascribed to both the different feedstock nature, pyrolysis temperature (lower in the case of PNS) and activation conditions, affecting the overall morphological properties [26]. The KOH activation had opposite effects on the surface areas of the two biomasses; for OMW the use of this porogen resulted in a lower surface area than the CO_2-activated samples, whereas for the PNS biomass we saw the highest surface area of any sample at 1970 m^2/g.

Table 2: Oxidizable carbon content (fixed + volatile matter) and BET surface area of resulting activated biochars

Sample	Oxidizable Carbon Content (Volatile + Fixed) wt%)	BET Surface Area (m^2/g)
OMW_1	0.82	742
OMW_2	0.87	444
OMW_3	0.80	658
PNS_4	0.93	1121
PNS_5	0.93	1970

Fourier Transform Infrared spectroscopy was used to identify the presence and nature of functional groups on the surface of the biochar samples (Figure 2). In agreement with previous reports, all samples displayed well-defined FTIR bands corresponding to vibrations of C-H bonds, as well as vibrations of bonds in oxygen and nitrogen functional groups [26-29].

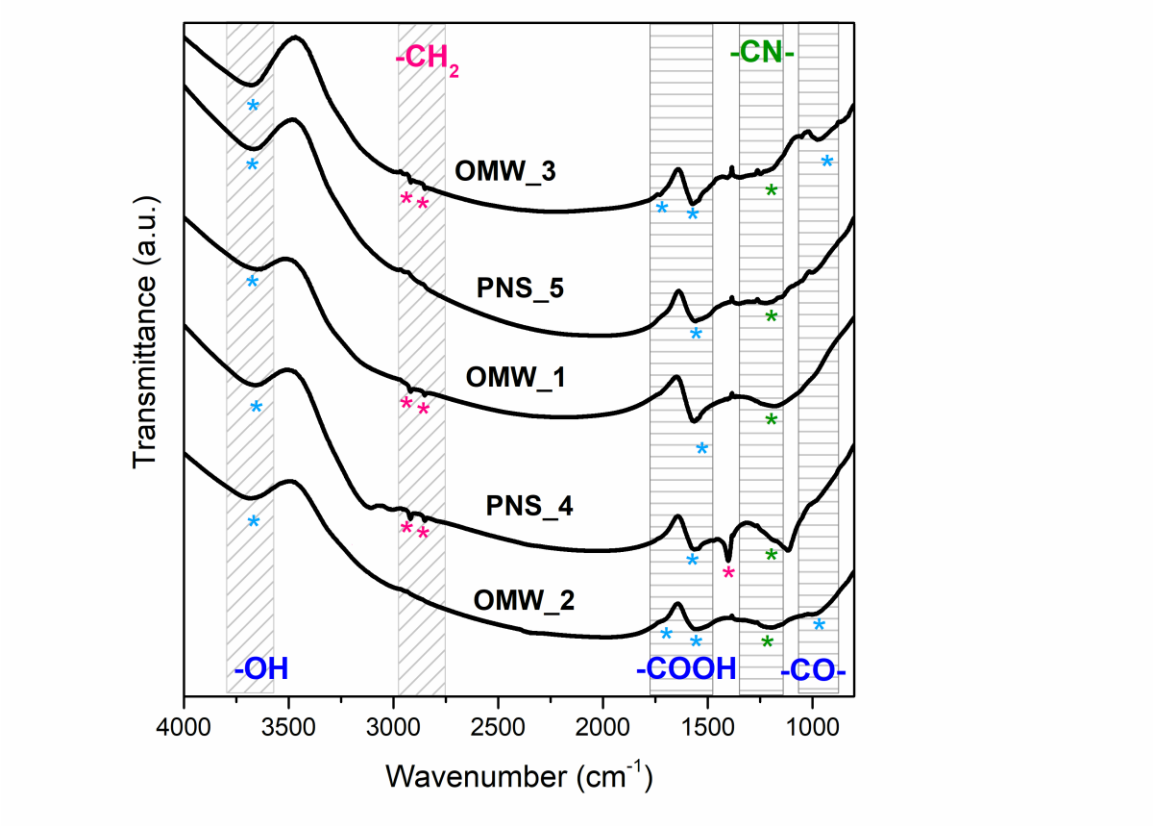

Figure 2. FTIR spectra of biochar carbon activated catalysts

Two vibration bands can be seen in the 2950-2850 cm^{-1} region for PNS_4, OMW_3, and OMW_1, which can be ascribed to the aliphatic C-H deforming vibration. Such bands are absent for PNS_5 and OMW_2. This is attributed to the effect of the KOH activating agent in aromatization of the product [30, 31]. In addition, PNS_4 presented a further intense peak at 1388 cm^{-1}, associated with the vibration of C-H bond in alkenes and alkyl groups. This finding suggests that the low temperature pyrolysis of the PNS_4 sample maintained the alkyl functional groups, compared to the other samples, which were pyrolyzed at higher temperature [17, 27].

The band at ~ 1200 cm^{-1}, visible for all samples, can be assigned to the asymmetric C-N stretching vibrations coupled with the out-of-plane NH_2, indicating the presence of

nitrogen functional groups in all samples [29]. The presence of nitrogen was further confirmed by elemental analysis results, which shows a nitrogen content ranging from 0.1 to 1.1 wt.%. In addition, all samples showed bands at 3660 cm^{-1} and 1570 cm^{-1} which can be assigned to OH and C=O stretching vibrations in carbonyl groups, respectively [32, 33]. Interestingly, OMW2 and OMW3 contain additional oxygen functional groups, as indicated by the two bands at 1730 cm^{-1} and 980 cm^{-1} arising from C=O stretching vibrations in carboxyl groups and alcoxy CO stretches [34]. Hence, the major difference in the functional groups of the biochar was the presence of an increased variety of oxygen functional groups (*i.e*, ether and carboxyl groups) in OMW2 and OMW3. As previously reported, such oxygen functional groups plays a key role in enhancing ORR activity of carbon-based materials [29].

3.2 Electrochemical characterization

The catalytic behaviour towards the oxygen reduction reaction (ORR) of the activated biochar samples was studied by cyclic voltammetry. Figure 3 shows CVs curves in N_2- and O_2-saturated neutral electrolyte solution for two representative samples of the series, i.e. OMW_3 and PNS_4, while CV curves for all samples are shown in Figure S2.

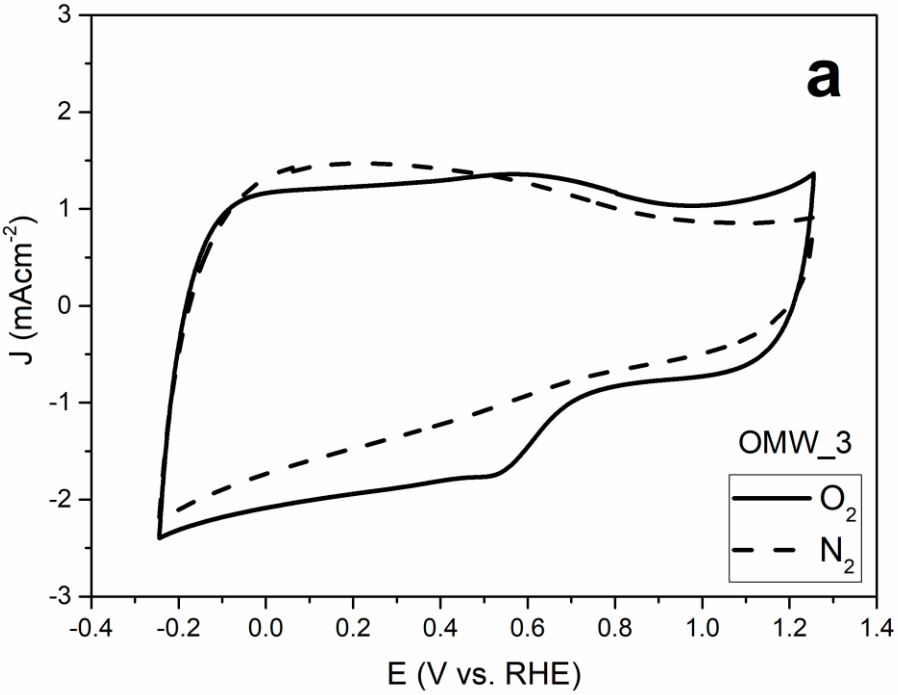
a
J (mAcm-2)
E (V vs. RHE)
OMW_3
O2
N2
3
2
1
0
-1
-2
-3
-0.4
-0.2
0.0
0.2
0.4
0.6
0.8
1.0
1.2
1.4

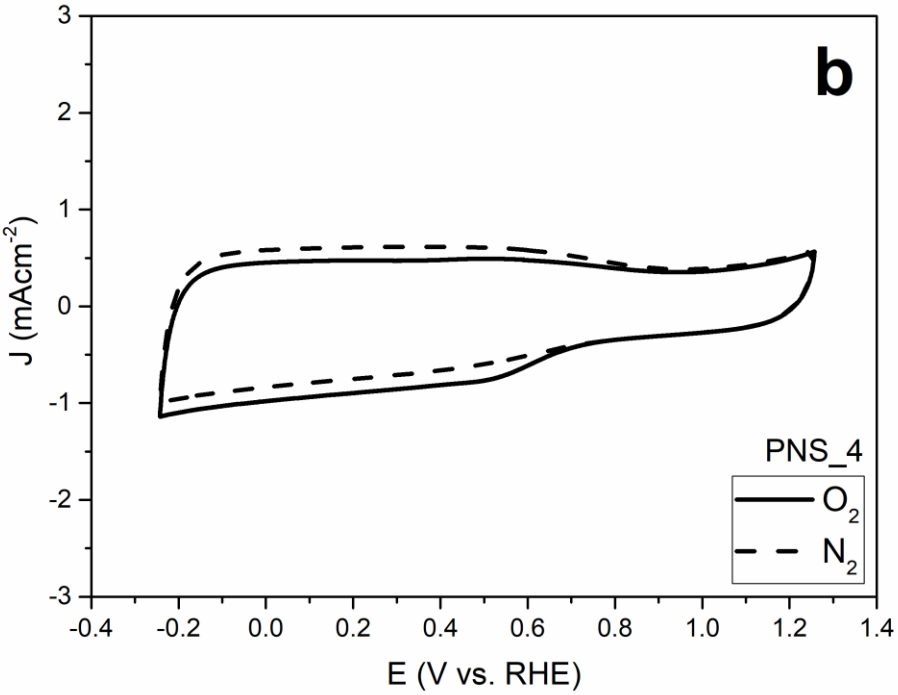
b
J (mAcm-2)
E (V vs. RHE)
PNS_4
O2
N2
3
2
1
0
-1
-2
-3
-0.4
-0.2
0.0
0.2
0.4
0.6
0.8
1.0
1.2
1.4

Figure 3: CV curves of OMW_3 (a) and PNS_4 (b) in O_2-saturated (solid line) and N_2-saturated (dash line) neutral PBS.

All samples showed the typical CV profile of high surface area carbon materials in N_2-saturated atmosphere (dashed curved in Figure 3), from which the double layer capacitance (CDL) and electrochemical surface area (ECSA) values were calculated, as illustrated in Table 3 and Figure S3. Biochar CDL values, showed in Table 3, were in good agreement with previous reports, especially considering variations due to synthesis and activation conditions [35-37]. ECSA values increased in the following order: PNS_4 < PNS_5 ≅ OMW_1 < OMW_2 < OMW_3. Despite their lower BET surface areas, OMW samples showed higher ECSA than that of PNS samples; in particular, OMW_2 and OMW_3 biochars showed the highest ECSA. This behaviour can be related to the increased hydrophilicity of OMW_2 and OMW_3 caused by their greater variety of oxygen functional groups, as revealed by FTIR. Along with hindering aggregation phenomena occurring during the electrode preparation in the ethanol-based ink [38], an increased hydrophilicity enhances electrode wettability and affinity of the electrolyte species for the electrocatalyst surface, resulting in a beneficial effect towards ORR [28, 39]. In the O_2-saturated atmosphere, a reduction peak centred in the 0.5-0.6 V vs. RHE can be seen for all samples (solid lines in Figure 3; additional CV curves in Figure S2), as a result of the catalytic activity towards ORR of the biochars. Peak potential (Epr) and peak current density (Jp) values are shown in Table 3. More positive Epr values corresponded to a higher reaction rate, such as higher absolute Jp values corresponded a greater density of active sites for oxygen adsorption. Among all samples, PNS_4 and PNS_5 samples show the poorest catalytic activity towards ORR, while OMW_2 and OMW_3 showed the highest performance, as revealed by the best set of Epr and Jpr results. The superior catalytic

activity of OMW_2 and OMW_3 can be ascribed to an interplay of surface chemistry and morphology, which lead to high surface area, high density of oxygen functional group and high hydrophilicity.

Table 3. Electrochemical parameters of biochar catalysts obtained by Cyclic Voltammetry and Linear Sweep Voltammetry under O_2 or N_2-saturated neutral PBS.

SAMPLE	Cyclic Voltammetry				Linear Sweep Voltammetry		
	J_{Pr} (mAcm^{-2})	E_{pr} (V vs. RHE)	C_{DL}/F m^{-2}	ECSA/m^{2}g^{-1}	E_{onset} (V vs. RHE) @1600 rpm	$E_{1/2}$ (V vs. RHE) @1600 rpm	n*e*- @ -0.35 V
OMW_1	0.35 ± 0.01	0.517 ± 0.00	107±2	119±2	0.76 ± 0.07	0.37 ± 0.05	2.9± 0.3
OMW_2	0.38 ± 0.03	0.627 ± 0.02	161±1	179±1	0.80 ± 0.02	0.44 ± 0.01	3.1±0.2
OMW_3	0.72 ± 0.25	0.537 ± 0.00	215±2	239±3	0.79 ± 0.03	0.42 ± 0.05	3.9±0.2
PNS_4	0.17 ± 0.02	0.517 ± 0.02	96.7±0.7	107±1	0.73 ± 0.10	0.33 ± 0.05	1.8±0.4
PNS_5	0.13 ± 0.01	0.477 ± 0.01	106±1	118±1	0.77 ± 0.02	0.30 ± 0.05	2.2±0.5

To gain deeper insight into the catalytic activity towards ORR of the biochars, linear sweep voltammetry (LSV) with rotating disk electrode (RDE) was carried out and is shown for OMW_3 (Figure 4a), as a representative sample of the series. The complete set of LSV curves for all samples is reported in Figure S4. The corresponding onset potential (E_{onset}) and half-wave potential ($E_{1/2}$) values are shown in Table 3. Both E_{onset} and $E_{1/2}$ for OMW_2 and OMW_3 are shifted towards more positive values, as compared to the other samples;

confirming their superior catalytic activity towards ORR, in good agreement with CV results. The number of electrons exchanged during ORR (n) can be also calculated according to the Koutecky-Levich (K-L) theory [4, 24]; K-L plots are shown in Figure 4b, and the resulting n values are listed in Table 3.

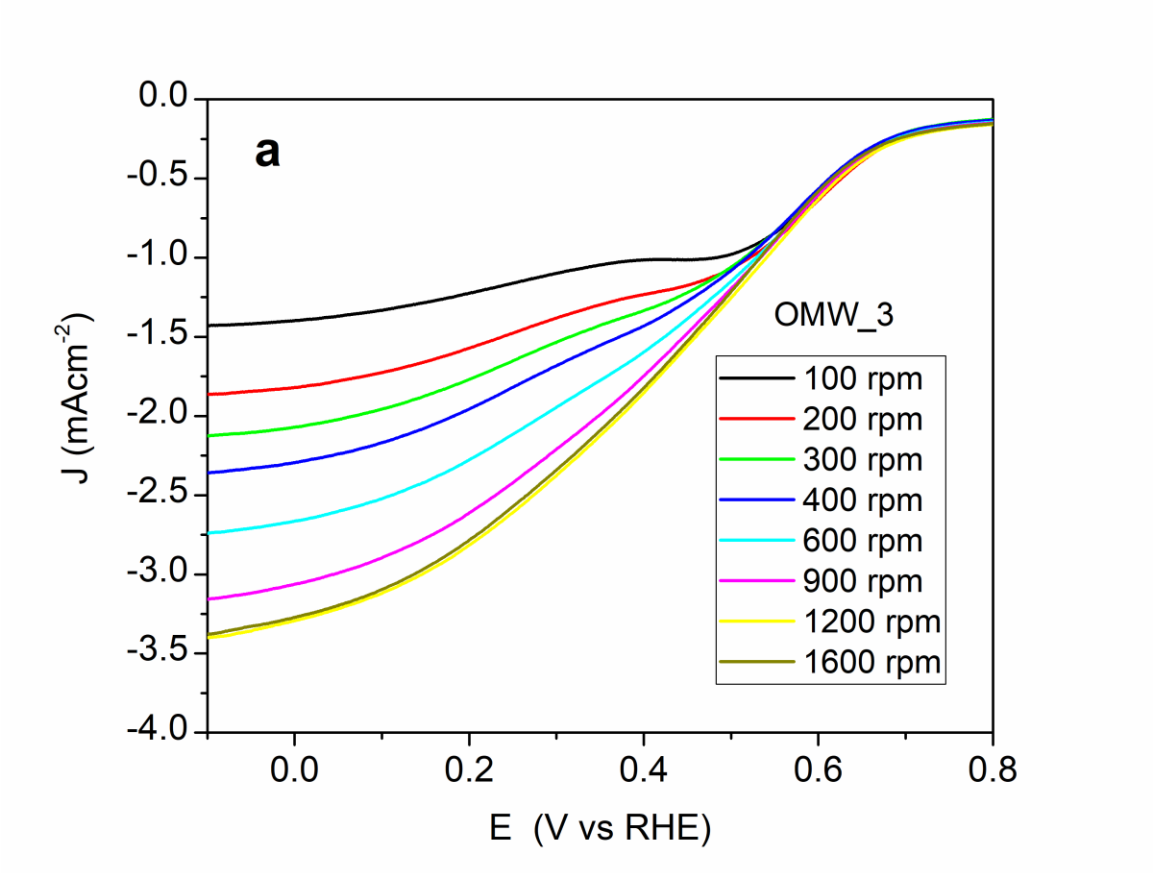

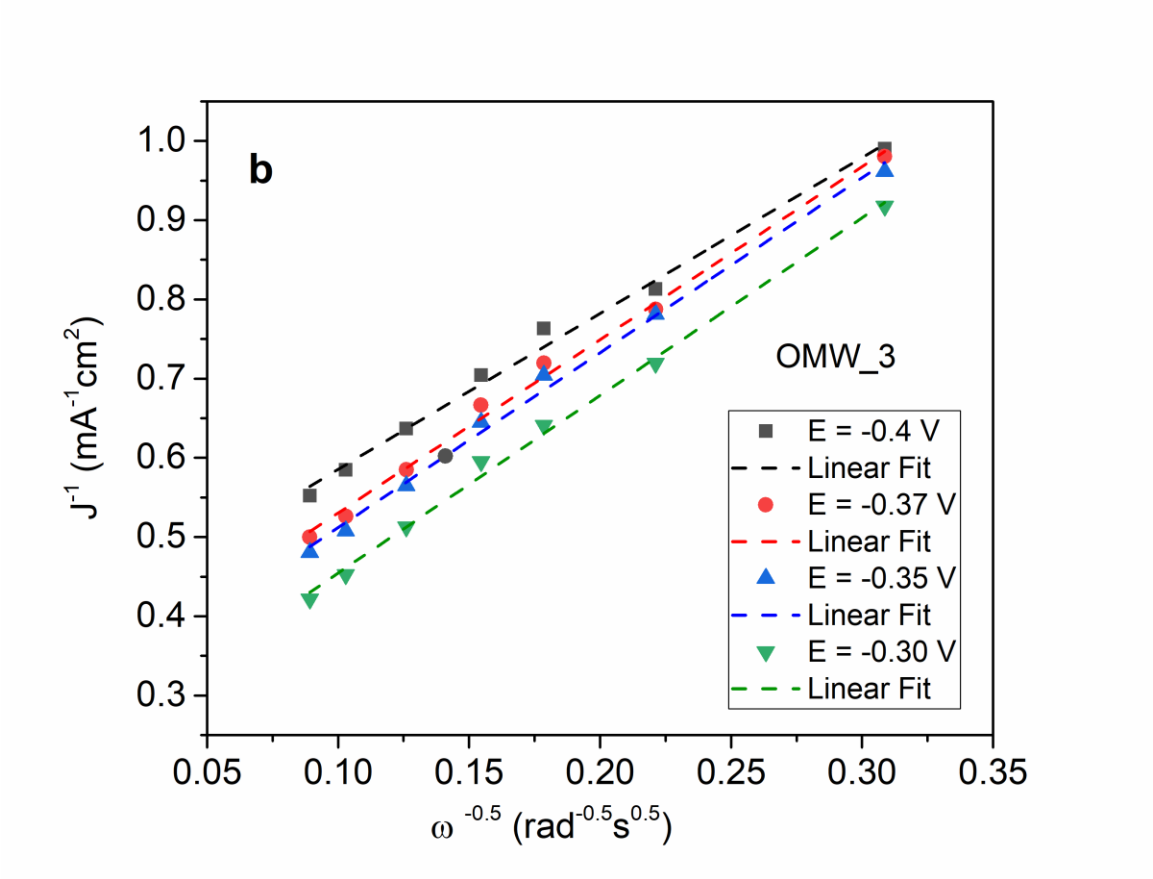

Figure 4: a) Background-corrected LSV-RDE curves acquired at electrode rotation speed from 100 to 1600 rpm for OMW_3; b) the corresponding K-L plots taken at different potential values.

KL plots, extrapolated at different potential values, show a good linearity in the 0.3 ÷ 0.4 V potential window. The number of electrons exchanged was higher for the OMW_3, OMW_2 and OMW_1 catalyst with a value of 3.9, 3.1 and 2.9, respectively. PNS_4 and PNS_5 catalysts showed the lowest number of electrons exchanged, lower and/or close to 2. In fact, when ORR takes place, oxygen can be reduced to water by either a direct 4-electron or a 2x2 electron transfer pathway, or to peroxide by a 2-electron pathway. For achieving high current density and avoiding peroxide formation, the water pathway is preferred [40]. The data in Table 3 indicate that ORR at the surface of PNS sample mainly

proceeds through the peroxide pathway, while the number of electrons exchanged during ORR at the surface of OMW_3 is close to 4, involving the 4 or 2x2 electron mechanisms as the possible pathway. On the other hand, OMW_1 and OMW_2 exhibit two coexisting pathways for ORR involving both the peroxide and water pathway.

The electrochemical characterization of the samples revealed that OMW_2 and OMW_3 showed the highest catalytic activity toward ORR in terms of reaction rate, density of active sites, and number of electrons exchanged, as a result of higher electrode double layer capacitance leading to the higher exposure of effective active sites.

These results are in good agreement with previous reports dealing with the study of ORR activity of biochar-based electrodes. Zhong et al. (2019) [11], investigated ORR activity of nitrogen-doped biochar derived from watermelon rind in alkaline media, demonstrating that a good ORR activity and an electron transfer number as high as 3.26 can be achieved owing to the high electrochemical active surface area of the sample. Similar findings were achieved by Marzorati et al. (2019) [41] who reported on electro-active biochar from pyrolysis of Giant Cane stalks; high surface electrocatalytic activity was sufficient to accelerate ORR at neutral pH, in terms of both onset potential (− 0.02 V vs Ag/AgCl) and limiting current density (0.1 mA cm^{-2}). Further studies on ORR performance of carbon-based catalysts found that the presence of oxygen and nitrogen groups on the carbon surface also plays a key role in accelerating ORR. In particular, Zhao et al. fabricated high performance graphitic carbon-based ORR electrocatalysts by crafting N-containing functional groups onto both holey graphene oxide and porous carbon obtained by thermal treatment of natural biomass [29, 34, 39]. The material treatment functionalized the carbon surface with a high density of oxygen-containing groups, which was critical for enhancing

oxygen electrocatalytic activity of this material in energy storage devices. In addition, the ORR performance was found to be dependent on crafted N groups, which. facilitate O_2 adsorption [42, 43].

3.3 Microbial fuel cell performance

Based on the physical-chemical and electrochemical characterizations, OMW_2 and OMW_3 were selected as materials for the cathode side of air-cathode MFCs to evaluate their performance under representative MFC operating conditions.

The performance of the Microbial fuel cells equipped with different cathodes was evaluated by monitoring the output voltage. Data obtained were compared with MFCs assembled using commercial carbon black as a control (CTRL). In total, 6 single chamber MFCs were used during the test. The cells were operated in parallel in batch mode using phosphate buffer solution 0.1M (PBS) and acetate (1 g L^{-1}) as the feed solution. The voltage output was monitored for approximately 480 h in order to evaluate the stable voltage production over time. As shown in Figure S5, after about 120h from inoculation, the MFCs achieved a stable output voltage; this acclimation time length is in line with those reported in the literature [44] showing that the biochars did not negatively affect the exoelectrogens bacteria growth. Concerning the maximum voltage generated, the bioreactors equipped with OMW_3 cathodes reached a maximum peak voltage of ≈0.4 V after 240 h. This maximum peak voltage was maintained roughly until the end of the test (Figure S4). The voltage output trend obtained from MFCs equipped with OMW_3 was compared with other MFC reactors equipped with OMW_2 biochar and the control. As reported in Figure S4, the voltages peaks obtained by the other cathodes, i.e. 0.12 V for OMW_2 and 0.13 V

for CTRL, were lower. From the voltage cycles peaks, the power density and polarizations curves were calculated in order to understand the maximum performance of the MFCs analyzed.

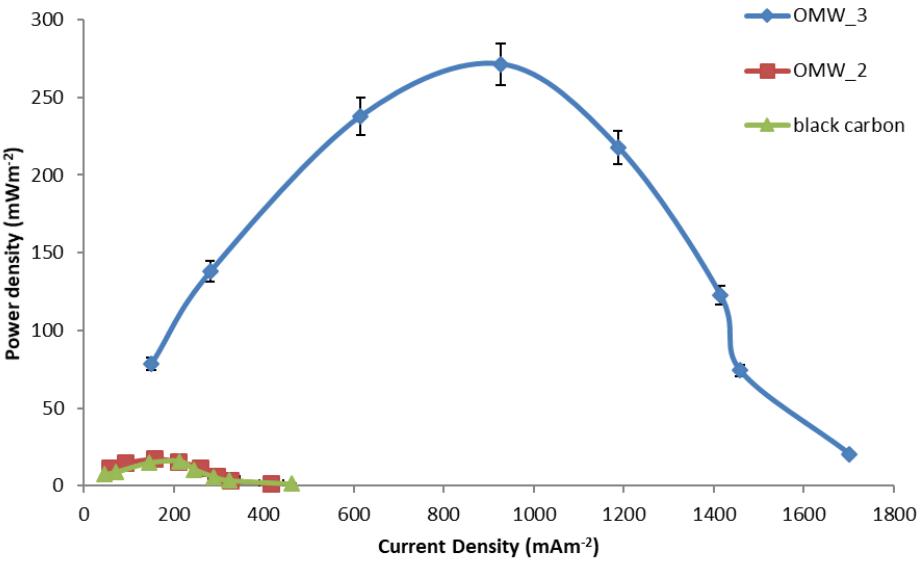

a

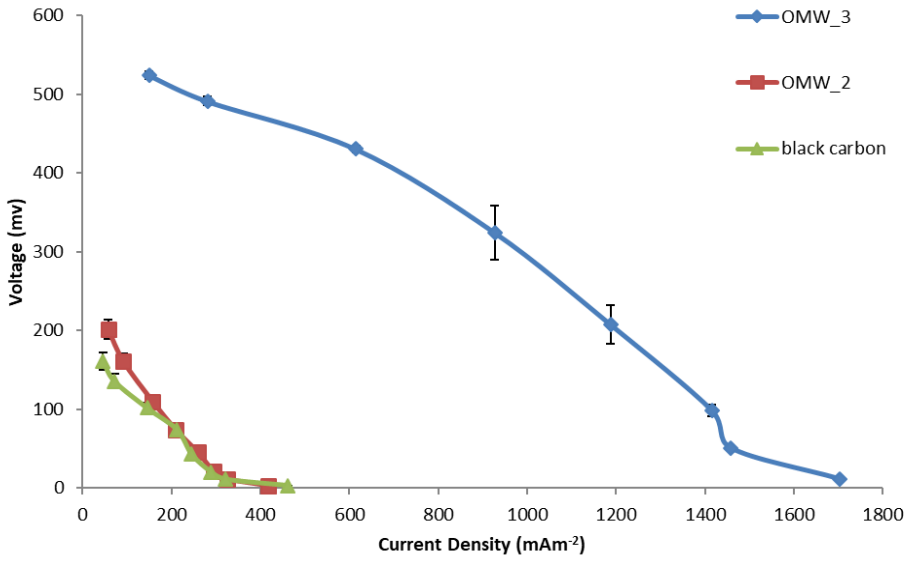

b

Figure 5: Power curves a) and polarization curves b) obtained from the MFCs reactors tested with OMW_3, OMW_2 biochars and black carbon (CTRL).

The power density and current density obtained from the MFC equipped with an OMW_3 cathode achieved a maximum power density of 271 ± 34 mWm^{-2} (R_{ext} 250 Ω) (Fig.5a, b) and a corresponding maximum volumetric power of 5 ± 0.75 Wm^{-3}. As indicated in Figure 5a the power density values from the OMW_3 cathode were about 15 times higher than the power density obtained from OMW_2 cathode (17.3 ± 1.5 mWm^{-2}) and the CTRL. This difference was also found by comparing the volumetric power (Table 4).

Table 4. Electrochemical parameters of biochar catalysts obtained by Cyclic Voltammetry and Linear Sweep Voltammetry under O_2 or N_2-saturated neutral PBS

Samples	E max (V)	Volumetric Power (Wm-3)	Coulombic Efficiency (C.E)
OMW_2	0.12 ± 0.01	0.55 ± 0.08	6.8 ± 1.0
OMW_3	0.37 ± 0.02	5.00 ± 0.65	9.9 ± 1.5
CTRL	0.13 ± 0.01	0.60 ± 0.10	8.1 ± 1.0

At last, the coulombic efficiency (CE) calculated for each cathode was compared (Table 3). The CE obtained from OMW_3 was 9.9 ± 1.5%, while for OMW_2 the value of CE was lower than MFCs modified with OMW_3 and CTRL. The results achieved during the microbial fuel cell test confirmed those obtained during the cyclic voltammetry experiments, where OMW_3 showed the highest ORR activity (Table 3). Data from the MFCs test were compared with results reported in literature. Li et al., (2018) [10] tested biochars derived from corncob as an oxygen reduction catalyst in the air cathode microbial fuel cells, obtaining a maximum output voltage and power density of 0.221 V and 0.458 Wm^{-3} respectively. Furthermore, Zhong et al., (2019) [11], reported MFC performances by using nitrogen-doped biochar derived from watermelon rind as oxygen reduction catalyst

in air cathode microbial fuel cells. In this case, a maximum output voltage of 0.27 V was achieved, corresponding to a maximum volumetric power of 0.262 Wm^{-3}. In both cases, data were comparable to the results obtained in this work, confirming that activated biochar obtained from olive mill waste is suitable as a catalyst for ORR in the air cathode of a microbial fuel cell.

4. Conclusions

Electrochemical characterization of biochar-based catalysts derived from olive mill waste and pistachio nut shells demonstrated good catalytic activity towards oxygen reduction reaction in neutral media. This beneficial catalytic activity is likely attributed to the wide variety of oxygen and nitrogen surface functionalities of the biochar and high electrochemical surface area; there was no distinct correlation of activity to oxidizable carbon content of the activated biochars. Microbial fuel cells equipped with biochar cathodes confirmed the results of the electrochemical tests. One activated biochar in particular – olive mill waste pyrolyzed at 600°C for 30 min, followed by CO_2 activation for 45 min at 800°C, achieved higher performance than conventional carbon black cathodes.

5. References

[1] T.G. Walmsley, H.Y.B. Ong, J.J. Klemeš, R.R. Tan, P.S. Varbanov, Circular Integration of processes, industries, and economies, Renew. Sust. Energ. Rev. 107 (2019) 507-515.

[2] J. Goldfarb, G. Dou, M. Salari, M.W. Grinstaff, Biomass-Based Fuels and Activated Carbon Electrode Materials: An Integrated Approach to Green Energy Systems, ACS Sustainable Chem. Eng. 5 (2017) 3046-3054.

[3] M. A. C. de Oliveira, B. Mecheri, A. D'Epifanio, E. Placidi, F. Arciprete, F. Valentini, A. Perandini, V. Valentini, S. Licoccia, Graphene oxide nanoplatforms to enhance catalytic performance of iron phthalocyanine for oxygen reduction reaction in bioelectrochemical systems, J. of Power Sources 356 (2017) 381-388.

[4] F. Shahbazi Farahani, B. Mecheri, M. Reza Majidi, M.A. C. de Oliveira, A. D'Epifanio, F. Zurlo, E. Placidi, F. Arciprete, S. Licoccia, MnOx-based electrocatalysts for enhanced oxygen reduction in microbial fuel cell air cathodes, J. of Power Sources, 390C (2018) 45-53.

[5] A. Iannaci, T. Pepè Sciarria, B. Mecheri, F. Adani, S. Licoccia, A. D'Epifanio, Power generation using a low-cost sulfated zirconium oxide based cathode in single chamber microbial fuel cells, J. Alloy Compd. 693 (2017) 170-176.

[6] C. Santoro, M. Kodali, S. Herrera, A. Serov, I. Ieropoulos, P. Atanassov, Power generation in microbial fuel cells using platinum group metal-free cathode catalyst: Effect of the catalyst loading on performance and costs, J. of Power Sources, 378 (2018) 169-175.

[7] C. Lv, B. Liang, M.S. Zhong, K. Li, Y. Qi, Activated carbon-supported multi-doped graphene as high-efficient catalyst to modify air cathode in microbial fuel cells, Electrochim. Acta 304 (2019) 360-369.

[8] B. Mecheri, V.C.A. Ficca, M.A. Costa de Oliveira, A. D'Epifanio, E. Placidi, F. Arciprete, & S. Licoccia, Facile synthesis of graphene-phthalocyanine composites as oxygen reduction electrocatalysts in microbial fuel cells, Applied Catalysis B: Environmental. 237 (2018) 699-707.

[9] Y. Wu, L. Wang, M. Jin, F. Kong, H. Qi, J. Nan, Reduced graphene oxide and biofilms as cathode catalysts to enhance energy and metal recovery in microbial fuel cell, Bioresour. Technol. 283 (2019) 129-137.

[10] M. Li, H. Zhang, T. Xiao, S. Wang, B. Zhang, D. Chen, M. Su, J. Tang, Low-cost biochar derived from corncob as oxygen reduction catalyst in air cathode microbial fuel cells, Electrochim. Acta 283 (2018) 780-788.

[11] K. Zhong, M. Li, Y. Yang, H. Zhang, B. Zhang, J. Tang, J. Yan, M. Su, Z. Yang, Nitrogen-doped biochar derived from watermelon rind as oxygen reduction catalyst in air cathode microbial fuel cells, Appl. Energy 242c (2019) 516-525.

[12] H. Yuan, L. Deng, Y. Qi, N. Kobayashi, J. Tang, Nonactivated and Activated Biochar Derived from Bananas as Alternative Cathode Catalyst in Microbial Fuel Cells, Sci. World J., (2014), 1-8.

[13] E. Agrafioti, G. Bouras, D. Kalderis, E. Diamadopoulos, Biochar production by sewage sludge pyrolysis. J. Anal. Appl. Pyrolysis 101 (2013) 72-78.

[14] S. Souilem, A. El-Abbassi, H. Kiai, A. Hafidi, S. Sayadi, C.M. Galanakis, Olive Mill Waste Recent Advances for Sustainable Management. In: C. M. Galanakis (Ed), Olive Mill Waste: Recent Advances for Sustainable Management, Academic Press, Elsevier, 2017, pp.1-28.

[15] T. Pepè Sciarria, A. Tenca, A. D'Epifanio, B. Mecheri, G. Merlino, M. Barbato, S. Borin, S. Licoccia, V. Garavaglia, F. Adani, Using olive mill wastewater to improve performance in producing electricity from domestic wastewater by using single-chamber microbial fuel cell, Bioresour. Technol. 147 (2013) 246-253.

[16] Nuts and dried fruits. Statistical Yearbook 2017/2018. INC: International nut and dried fruit council. https://www.nutfruit.org/industry/technical-resources, 2017 (accessed 20 December 2019)

[17] J. L. Goldfarb, L. Buessing, E. Gunn, M. Lever, A. Billias, E. Casoliba, A. Schievano, F. Adani, Novel Integrated Biorefinery for Olive Mill Waste Management: Utilization of Secondary Waste for Water Treatment, ACS Sustainable Chem. Eng. 5 (2017) 876−884.

[18] Y. Lu, N. Zhu, F. Yin, T. Yang, P. Wu, Z. Dang, M. Liu, X. Wei, Biomass-derived heteroatoms-doped mesoporous carbon for efficient oxygen reduction in microbial fuel cells, Biosens. Bioelectron. 98 (2017) 350-356.

[19] B. Mecheri, A. Iannaci, A. D'Epifanio, A. Mauri, S. Licoccia, Facile synthesis of graphene-phthalocyanine composites as oxygen reduction electrocatalysts in microbial fuel cells, Chem. Plus. Chem. 81 (2016) 80-85.

[20] C. Santoro, C. Arbizzani, B. Erable, I. Ieropoulos, Microbial fuel cells: From fundamentals to applications. A review, J. of Power Sources 356 (2017) 225-244.

[21] E. Frackowiak, Carbon materials for supercapacitor application, Phys. Chem. Chem. Phys. 9 (2007) 1774.

[22] M.A.C de Oliveira, V.C.A. Ficca, R. Gokhale, et al., Iron(II) phthalocyanine (FePc) over carbon support for oxygen reduction reaction electrocatalysts operating in alkaline electrolyte, J. Solid State Electrochem (2020). https://doi.org/10.1007/s10008-020-04537-x

[23] X. Yin, H. T. Chung, U. Martinez, L. Lin, K. Artyushkova, and P. Zelenay, PGM-free ORR catalysts designed by templating PANI-type polymers containing functional groups with high affinity to iron, J. Electrochem. Soc. 166 (2019) F3240-F3245.

[24] M.-T. Nguyen, B. Mecheri, A. Iannaci, A. D'Epifanio, S. Licoccia, Iron/Polyindole-based Electrocatalysts to Enhance Oxygen Reduction in Microbial Fuel Cells, Electrochim. Acta 190 (2016) 388-395.

[25] A. Iannaci, B. Mecheri, A. D'Epifanio, M.J. Lázaro Elorri, S. Licoccia, Iron–nitrogen-functionalized carbon as efficient oxygen reduction reaction electrocatalyst in microbial fuel cells, Int. J. Hydrogen Energ. 41 (2016) 19637-19644.

[26] Y. Yuan, T. Yuan, D. Wang, J. Tang, S. Zhou, Sewage sludge biochar as an efficient catalyst for oxygen reduction reaction in a microbial fuel cell, Bioresour. Technol. 144 (2013) 115-120.

[27] K. Komnitsas, D. Zaharaki, I. Pyliotis, D. Vamvuka, G. Bartzas, Assessment of Pistachio Shell Biochar Quality and Its Potential for Adsorption of Heavy Metals, Waste Biomass. Valor. 6 (2015) 805-816.

[28] K. Kordek, L. Jiang, K. Fan, Z. Zhu, L. Xu, M. Al-Mamun, Y. Dou, S. Chen, P. Liu, H. Yin, P. Rutkowski, H. Zhao, Two-Step Activated Carbon Cloth with Oxygen-Rich Functional Groups as a High-Performance Additive-Free Air Electrode for Flexible Zinc–Air Batteries, Adv. Energy Mater. 9 (2019) 1802936.

[29] X. Liu, L. Jiang, Z. Zhu, S. Chen, Y. Dou, P. Liu, Y. Wang, H. Yin, Z. Tang, H. Zhao, Wet-chemistry grafted active pyridinic nitrogen sites on holey graphene edges as high performance ORR electrocatalyst for Zn-Air batteries, Mater. Today Energy 11 (2019) 24-29.

[30] R. Azargohar, A. K. Dalai, Biochar is a precursor of activated carbon, Appl. Biochem. Biotech. 131 (2006) 762-773.

[31] H. Jin, X. Wang, Z. Gu, J. Polin, Carbon materials from high ash biochar for supercapacitor and improvement of capacitance with HNO_3 surface oxidation, J. of Power Sources 236 (2013) 285-292.

[32] K. Mustafa, M.K. Hossain, V. Strezov, K. Yin Chan, A. Ziolkowski, P.F. Nelson, Influence of pyrolysis temperature on production and nutrient properties of wastewater sludge biochar, J. Environ. Manage. 92 (2011) 223-228.

[33] T. Siengchum, M. Isenberg, S S.C. Chuang, Fast pyrolysis of coconut biomass – An FTIR study, Fuel 105 (2013) 559–565.

[34] H. Zhang, J. Chen, Y. Li, P. Liu, Y. Wang, T. An, H. Zhao, Nitrogen-Doped Carbon Nanodots@Nanospheres as An Efficient Electrocatalyst for Oxygen Reduction Reaction, Electrochim. Acta 165 (2015) 7–13.

[35] L.-H. Wang, M. Toyoda, M. Inagaki, Dependence of electric double layer capacitance of activated carbons on the types of pores and their surface areas, New Carbon. Mater. 23 (2008) 111-115.

[36] A.M. Dehkhoda, N. Ellis, E. Gyenge, Electrosorption on activated biochar: effect of thermo-chemical activation treatment on the electric double layer capacitance, J. Appl. Electrochem. 44 (2014) 141–57.

[37] M. Genovese, J. Jiang, K. Lian, and N. Holm, High capacitive performance of exfoliated biochar nanosheets from biomass waste corn cob, J. Mater. Chem. A 3 (2015) 2903-2913.

[38] M. Gray, M. G. Johnson, M. I. Dragila, M. Kleber, Water uptake in biochars: The roles of porosity and hydrophobicity, Biomass Bioenerg. 61 (2014) 96-205.

[39] C. Zhao, G. Liu, N. Suna, X. Zhang, G. Wanga, Y. Zhanga, H. Zhang, H. Zhao, Biomass-derived N-doped porous carbon as electrode materials for Zn-airbattery powered capacitive deionization, Chem. Eng. J. 334 (2018) 1270–1280.

[40] B. Erable, D. Féron, A. Bergel, Microbial catalysis of the oxygen reduction reaction for microbial fuel cells: a review, Chem. Sus. Chem. 5 (2012) 975-87.

[41] S. Marzorati, A. Goglio, S. Fest-Santini, D. Mombelli, F. Villa, P. Cristiani, A. Schievano, Air-breathing bio-cathodes based on electro-active biochar from pyrolysis of Giant Cane stalks, Int. J. Hydrog. Energy 44 (2019) 4496-4507.

[42] N. Sun, X. Zhang, C. Zhao, H. Wang, H. Lu, S. Kang, H. Zhou, H. Zhang, H. Zhao, G. Wang, Three-Dimensional N-doped Porous Carbon Derived from Monosodium

Glutamate for Capacitive Deionization and the Oxygen Reduction Reaction, ChemElectroChem, 5 (2018) 3873-3880.

[43] Y. Zhao, J. Wan, H. Yao, L. Zhang, K. Lin, L. Wang, N. Yang, D. Liu, L. Song, J. Zhu, L. Gu, L. Liu, H. Zhao, Y. Li, D. Wang, Few-layer graphdiyne doped with sp-hybridized nitrogen atoms at acetylenic sites for oxygen reduction electrocatalysis, Nat. Chem. 10 (2018) 924-931.

[44] G. Liu, M.D. Yates, S. Cheng, D.F. Call, D. Sun, B.E. Logan, Examination of microbial fuel cell start-up times with domestic wastewater and additional amendments, Bioresour. Technol. 102 (2011) 7301–7306.